Homodyne laser Doppler vibrometer on silicon-on-insulator with integrated 90 degree optical hybrids

Yanlu Li* **and Roel Baets**

Photonics Research Group, Department of Information Technology (INTEC), Ghent-University – IMEC, Sint-Pietersnieuwstraat 41, 9000 Ghent, Belgium, Center for Nano - and Biophotonics (NB-Photonics), Ghent University, Sint-Pietersnieuwstraat 41, 9000 Ghent, Belgium

*Yanlu.Li@intec.ugent.be

Abstract: A miniaturized homodyne laser Doppler vibrometer (LDV) with a compact 90° optical hybrid is experimentally demonstrated on a CMOS compatible silicon-on-insulator (SOI) platform. Optical components on this platform usually have inadequate suppressions of spurious reflections, which significantly influence the performance of the LDV. Numerical compensation methods are implemented to effectively decrease the impact of these spurious reflections. With the help of these compensation methods, measurements for both super-half-wavelength and sub-half-wavelength vibrations are demonstrated. Results show that the minimal detectable velocity is around 1.2 μm/s.

OCIS codes: (280.3340) Laser Doppler velocimetry; (130.6750) Systems.

References and links

1. P. Castellini, M. Martarelli, and E. P. Tomasini, "Laser Doppler vibrometry: development of advanced solution answering to technology's needs," Mech. Syst. Signal. Proc. **20**, 1265–1285 (2006).
2. J. W. Czarske, "Laser Doppler velocimetry using powerful solid-state light sources," Meas. Sci. Technol. **17**, R71–R91 (2006).
3. A. T. Waz, P. R. Kaczarek, and K. M. Aramski, "Laser-fibre vibrometry at 1550 nm," Meas. Sci. Technol. **20**, 105301 (2009).
4. S. M. Khanna, "Homodyne interferometer for basilar membrane measurements," Hearing Res. **23**, 9-26 (1986).
5. J. La, S. Wang, K. Kim, and K. Park, "High-speed FM demodulator of a homodyne laser interferometer for measuring mechanical vibration," Opt. Eng. **43**(6), 1341–1349 (2004).
6. R. Halir, G. Roelkens, and A. Ortega-Moñux, and J. G. Wangüemert-Pérez, "High-performance 90° hybrid based on a silicon-on-insulator multimode interference coupler," Opt. Lett. **36**, 178–180 (2011).
7. W. Bogaerts, R. Baets, P. Dumon, V. Wiaux, S. Beckx, D. Taillaert, B. Luyssaert, J. Van Campenhout, P. Bienstman, and D. Van Thourhout "Nanophotonic waveguide in silicon-on-insulator fabricated with CMOS technology," J. Lightwave Technol. **23**, 401–402 (2005).
8. S. Selvaraja, W. Bogaerts, and D. Van Thourhout, "Loss reduction in silicon nanophotonic waveguide microbends through etch profile improvement," Opt. Commun. **284**, 2141–2144 (2011).
9. H. Yu, W. Bogaerts, and A. De Keersgieter, "Optimization of ion implantation condition for depletion-type silicon optical modulators," IEEE J. Quantum. Elect. **46**, 1763–1768 (2010).
10. L. Vivien, M. Rouvière, J-M Fédéli, D. Marris-Morini, J.-F. Damlencourt, J. Mangeney, P. Crozat, L. El Melhaoui, E. Cassan, X. Le Roux, D. Pascal, and S. Laval, "High speed and high responsivity germanium photodetector integrated in a Silicon-On-Insulator microwaveguide," Opt. Express **15** 9843–9848 (2007).
11. S. Stankovic, J. Richard, M. N. Sysak, J. M. Heck, G. Roelkens, and D. Van Thourhout, "Hybrid III-V/Si distributed-feedback laser based on adhesive bonding," IEEE Photon. Technol. Lett. **24**, 2155–2158 (2012).
12. S. Ghosh, S. Keyvaninia, Y. Shoji, W. Van Roy, T. Mizumoto, G. Roelkens, and R. Baets, "Compact Mach-Zehnder interferometer Ce:YIG/SOI optical isolators," IEEE Photon. Technol. Lett. **24**, 1653–1656 (2012).

#187527 - $15.00 USD Received 21 Mar 2013; revised 14 May 2013; accepted 16 May 2013; published 24 May 2013

13. Y. Li, S. Verstuyft, G. Yurtsever, S. Keyvaninia, G. Roelkens, D. Van Thourhout, and R. Baets, "Heterodyne laser Doppler vibrometers integrated on silicon-on-insulator based on serrodyne thermo-optic frequency shifters," Appl. Opt. **52**, 2145–2152 (2013).
14. K. G. Krauter, G. F. Jacobson, J. R. Patterson, J. H. Nguyen, and W. P. Ambrose, "Single-mode fiber, velocity interferometry," Rev. Sci. Instrum. **82**, 045110 (2011).
15. Y. Li, D. Vermeulen, Y. De Koninck, G. Yurtsever, G. Roelkens, and R. Baets, "Compact grating couplers on silicon-on-insulator with reduced backreflection," Opt. Lett. **37**, 4356–4358 (2012).
16. Y. Li, L. Li, B. Tian, G. Roelkens, and R. Baets, "Reflectionless tilted grating couplers with improved coupling efficiency based on a silicon overlay," to be published.
17. http://www.epixfab.eu

1. Introduction

A laser Doppler vibrometer (LDV) deploys the optical coherent detection method to retrieve the instantaneous velocities of a vibrating surface. A major advantage of LDVs over traditional vibration sensors (e.g. accelerometers) is their ability to perform non-intrusive vibration measurements, which helps to reduce the effect of accelerometer mass loading [1,2]. Therefore, LDVs have been widely exploited in a variety of application areas, such as mechanical engineering and biomedicine. Two types of LDVs, namely the heterodyne LDV and the homodyne LDV, are typically used to measure single point vibrations. In the heterodyne LDV, an optical frequency shifter (OFS) is required to ensure that the carrier of the photocurrent signal (before demodulation) does not lie in a low frequency region, where the influence of 1/f noise is significant [3]. In the homodyne LDV, however, the OFS is not included, so it is usually not as sensitive as the heterodyne LDV. In order to improve the measurement sensitivity of homodyne LDVs, different detection techniques have been developed, in which a quadrature demodulation approach with a 90° optical hybrid is frequently used [4–6]. The quadrature demodulation helps to determine the direction of the motion and to reduce the influence of power fluctuations from the laser source, indicating a sensitivity improvement and a demodulation complexity reduction.

Many applications require an adequate miniaturization of the LDV, so the device size is a major concern in LDV designs. In this paper, we propose a miniaturized photonic integrated circuit (PIC) based LDV on a CMOS compatible silicon-on-insulator (SOI) platform [7]. Most optical components required in an LDV have been realized on this platform, e.g. low loss optical waveguides [8], high speed phase modulators [9], high speed photo-detectors [10], adhesive bonded distributed-feedback (DFB) lasers [11], and integrated optical isolators [12]. Thanks to the small bend radius of the optical waveguide and the weak bend loss of the guided mode (typically 0.03 dB/90° for a bend with 2 μm radius [8]) on this SOI platform, the size of the PIC-based LDV can be dramatically lower than that of more conventional implementations. E.g. the footprint of the homodyne LDV demonstrated in this paper is less than 1 mm^2. In addition, the high-volume production cost of the PIC-based LDVs can also be dramatically reduced in this CMOS compatible SOI platform.

We have reported a heterodyne LDV on the SOI platform with a thermo-optic OFS [13], but the detectable frequency range of such an LDV is limited by the frequency of the OFS. Therefore, we propose a new homodyne LDV on the SOI platform. This homodyne LDV is suitable for measuring vibrations with large amplitudes or high accelerations (e.g. high pressure shock-waves [14]), which may be beyond the measurement range of a heterodyne LDV. In addition, the fabrication of the homodyne LDV is simple due to the absence of OFS.

Several issues for homodyne LDVs on the SOI platform will be addressed in this paper, including the influence of unbalanced detection efficiencies of the photo-detectors, imperfect 90° optical hybrids, and on-chip spurious reflections. In the following sections, we will first analyze these problems theoretically and introduce an approach to compensate their impact on

#187527 - $15.00 USD Received 21 Mar 2013; revised 14 May 2013; accepted 16 May 2013; published 24 May 2013

the LDV outputs. The measurement results of fabricated homodyne LDVs will be reported and analyzed afterwards. Finally conclusions are drawn.

2. Theory of homodyne LDVs

The optical part of an on-chip homodyne LDV with a 90° optical hybrid is usually implemented based on a Mach-Zehnder interferometer, which is schematically shown in Fig. 1. It comprises a laser source, an optical isolator, a 3 dB optical splitter (os1), two optical arms (a measurement arm and a reference arm), a 90° optical hybrid and two pairs of balanced photo-detectors (BPDs). The optical splitters and the 90° optical hybrid are realized with rib waveguide based multi-mode interference (MMI) couplers. Particularly, the 90° optical hybrid is a special 2x4 MMI coupler reported by Halir *et al.* [6], of which the four output ports have the exact phase relation that is required in a 90° optical hybrid. In order to couple light from the PIC-based LDV to the vibrating target and pick up the back-reflected light which carries the velocity information of the target, an optical coupler (oc) combined with an optical splitter (os2) is placed in the measurement arm (see Fig. 1). The optical coupler (oc) is designed to have a high coupling efficiency combined with a low back reflection [15, 16]. Another coupling configuration with two optical couplers can also be utilized, which will be explained later. Assisted by an imaging optical system, the out-coupled measurement light (λ_0 = 1550 nm) is focused on the vibrating target. A portion of the reflected light is picked up by the LDV and is then recombined with the reference signal in the optical hybrid. In order to solely test the functionality of the passive interferometer of the homodyne LDV, the light source (a DFB laser) and the detectors are implemented externally in the work reported in this paper and connected with the chip via a fiber array (see Fig. 1).

Assume that the reference signal is expressed as $E_r(t) = rE_0(t)\exp(i2\pi f_0 t)$ and the measurement signal is $E_m(t) = m(t)E_0(t)\exp\{i[2\pi f_0 t + \theta_D(t)]\}$, where f_0, $E_0(t)$ are the frequency and amplitude of the light signal before it is sent to the optical splitter os1, respectively, $rE_0(t)$ and $m(t)E_0(t)$ are the amplitudes of the reference and measurement signals, respectively, and $\theta_D(t)$ is the Doppler phase shift of the measurement light caused by the vibration of the target, which is expressed as $\theta_D(t) = 2\pi\int 2v(t)/\lambda_0 dt$, where $v(t)$ is the instantaneous velocity of the surface and λ_0 is the vacuum wavelength of the light. The four output signals of the 90° optical hybrid are expressed as

$$\begin{pmatrix} E_1(t) \\ E_2(t) \\ E_3(t) \\ E_4(t) \end{pmatrix} = \begin{pmatrix} \kappa_{1,1} & \kappa_{1,2}e^{i\phi_{1,2}} \\ \kappa_{2,1} & \kappa_{2,2}e^{i\phi_{2,2}} \\ \kappa_{3,1} & \kappa_{3,2}e^{i\phi_{3,2}} \\ \kappa_{4,1} & \kappa_{4,2}e^{i\phi_{4,2}} \end{pmatrix} \begin{pmatrix} E_r(t) \\ E_m(t) \end{pmatrix}, \tag{1}$$

For an ideal 90° optical hybrid, $\kappa_{j,k} = 1/2$ for all j,k values, and $\phi_{j,2} = 0, \pi, \pi/2, 3\pi/2$ for

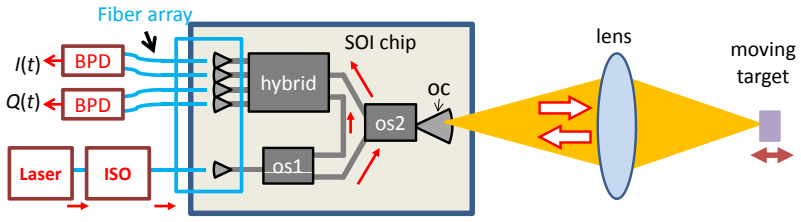

Fig. 1. The schematic show of a typical homodyne LDV. In this figure, *ISO* stands for optical isolator, *BPD* stands for balanced photo detector, *oc* stands for optical coupler, *os1* and *os2* stand for two optical splitters, and *hybrid* stands for 90° optical hybrid.

#187527 - $15.00 USD Received 21 Mar 2013; revised 14 May 2013; accepted 16 May 2013; published 24 May 2013

$j = 1,2,3,4$, respectively. The corresponding photo-current signals are thus expressed as $i_j(t) = \eta_j |E_j(t)|^2$, where η_j is the detection efficiency of each photo detector. If the 90° optical hybrid is ideal and the detection efficiencies of the detectors are identical (i.e. $\eta_j = \eta$ for all j values), the outputs of the two balanced photo-detectors can thus be expressed as

$$I(t) \equiv i_1(t) - i_2(t) = \eta E_0^2(t) rm(t) \cos[\theta_D(t)] \quad (2)$$

$$Q(t) \equiv i_3(t) - i_4(t) = \eta E_0^2(t) rm(t) \sin[\theta_D(t)]. \quad (3)$$

$I(t)$ and $Q(t)$ describe a circular Lissajous curve. With these two signals, the instantaneous Doppler phase shift $\theta_D(t)$ can be recovered by calculating the value of $\arctan[Q(t)/I(t)]$ with the help of a digital signal processing (DSP) approach. It can be found that the variations from the terms of $E_0(t)$ and $m(t)$ are removed with this method.

In practice, there are still several problems in an on-chip homodyne LDV. Firstly, due to the misalignment of the fiber array, the detection efficiencies η_j of the photo detectors may be different from each other. Secondly, the 90° optical hybrid may not work ideally due to deviations both in design and in fabrication. Thirdly, some significant on-chip spurious reflections may be mixed with the useful measurement signal and deteriorate the outputs. For instance, a spurious reflection can be introduced in the optical splitter os2 (see Fig. 1). Considering these deviations, the output photo-current signals should be written as

$$i_j(t) = C_j(t) + S_j(t) + R(t), \quad (4)$$

where

$$C_j(t) = \zeta_j(t)[\kappa_{j,1}^2 r^2 + \kappa_{j,2}^2 m^2(t)] \quad (5)$$

$$S_j(t) = 2\zeta_j(t)\kappa_{j,1}\kappa_{j,2} m(t) r \cos[\theta_D(t) + \phi_{j,2}], \quad (6)$$

with $\zeta_j(t) = \eta_j E_0^2(t)$, and $R(t)$ is introduced by spurious reflections and has a form $A + B\cos(\theta_D(t) + C)$.

It can be found that both $I(t)$ and $Q(t)$ can also be simplified to the form $A + B\cos(\theta_D(t) + C)$ even when strong spurious reflections are mixed with the useful signals. Since these two signals share the same frequency with respect to the variable $\theta_D(t)$, the Lissajous curve generated from these signals turns out to be an ellipse. Consequently, $I(t)$ and $Q(t)$ can be expressed as

$$I(t) = I_0 + a\cos[\theta_D(t) + \varphi_1]\cos(\varphi_0) - b\sin[\theta_D(t) + \varphi_1]\sin(\varphi_0) \quad (7)$$

$$Q(t) = Q_0 + a\cos[\theta_D(t) + \varphi_1]\sin(\varphi_0) + b\sin[\theta_D(t) + \varphi_1]\cos(\varphi_0), \quad (8)$$

where (I_0,Q_0) is the center position of the ellipse, φ_0 is the inclination angle, φ_1 is a constant phase shift, a and b are the semi-major and semi-minor axes of the ellipse, respectively.

When the amplitude of the measured vibration is larger than $\lambda_0/2$, a compensation approach can proceed as follow: (1) the parameters (I_0, Q_0, a, b, and φ_0) of the measured I&Q trace are obtained with a numerical method. (2) the center of the I&Q ellipse is shifted to the origin according to the following algorithm

$$I_1(t) = I(t) - I_0$$

$$Q_1(t) = Q(t) - Q_0. \quad (9)$$

(3) The ellipse is then transformed to a circle by using the following formula

$$I'(t) = b[I_1(t)\cos(\varphi_0) + Q_1(t)\sin(\varphi_0)] \quad (10)$$

$$Q'(t) = a[-I_1(t)\sin(\varphi_0) + Q_1(t)\cos(\varphi_0)]. \quad (11)$$

#187527 - $15.00 USD Received 21 Mar 2013; revised 14 May 2013; accepted 16 May 2013; published 24 May 2013

The eventually achieved trace of $(I'(t),Q'(t))$ is a circle with a radius of ab. The aforementioned arc-tangent approach can then be used to calculate the Doppler phase shift. The retrieved phase in this case is the sum of the desired Doppler phase shift $\theta_D(t)$ and a constant phase shift φ_1. Since this φ_1 is a constant value and is not important for the outputs, it can be omitted.

However, fluctuations in the light amplitude is hardly avoidable, resulting in variations of the compensation parameters (I_0, Q_0, a, b and φ_0). To solve this problem, one can use an active compensation approach, in which the five compensation parameters are measured and updated at regular intervals. With this approach, the changes of these compensation parameters can be tracked. However, when the vibrating amplitude is less than $\lambda_0/2$, the I&Q trace will become an incomplete ellipse, thus the five compensation parameters will be unachievable. An improved active compensation approach can be used in this case, in which an assumption is made that the only deviation source is the change of $E_0(t)$. A calibration measurement on a large vibration should be done in the beginning to obtain the initial five parameters. After the initializing calibration, the target vibration with a small amplitude is measured and the average of $I(t)$ and $Q(t)$ are tracked. The measured variations of these average values can be used to calculate the changes of the other compensation parameters. This method should be done when the temperature of the chip and the wavelength of the laser source is stabilized. The active compensation approach also requires more calculating time, and hence it may not be suitable for measuring vibrations with higher frequencies.

The impact of wavelength and temperature variations on the 90° optical hybrid have also been assessed by simulation with the commercial FimmWave mode solver. It can be found that the $\kappa_{j,k}$ and $\phi_{j,2}$ of the 90° optical hybrid change slowly with wavelength. When the wavelength increases from 1545 nm to 1555 nm, the maximal changes of $\kappa_{j,k}$ and $\phi_{j,2}$ are small values of 4% and 4°, respectively. The influence of the temperature is also very weak. For a temperature change of 20°C in simulation, the maximal change of $\kappa_{j,k}$ is 0.3%, and the maximal phase deviation $\phi_{j,2}$ is 0.3°. These results indicate that the hybrid itself is insensitive to the wavelength and temperature variations. However, the stability of the whole PIC is not only influenced by the 90° optical hybrid. The spurious reflections in the PIC vary strongly with wavelength and temperature, resulting in a strong influence on the stability of the LDV. Hence, to alleviate the output deviations, efforts should be focused on the suppression of on-chip spurious reflections.

3. Results and discussions

A number of on-chip homodyne LDVs with compact 90° optical hybrids are fabricated using 193 nm deep ultra-violet lithography through ePIXfab (advanced passive process module) [17]. Since the top silicon layer is only 220 nm thick, a rib waveguide can be realized by forming

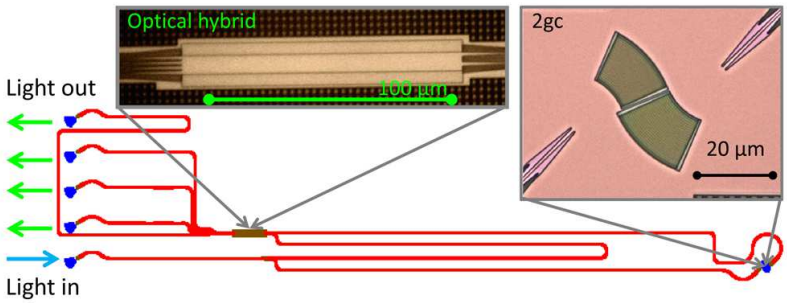

Fig. 2. The PIC design and microscope images of the 90° optical hybrid and of the 2gc light receiving components.

#187527 - $15.00 USD Received 21 Mar 2013; revised 14 May 2013; accepted 16 May 2013; published 24 May 2013

two adjacent silicon trenches (220 nm deep or 70 nm deep) with a small spacing (e.g. 450 nm) in the top silicon layer using several processes including lithography and dry etching. The high index contrast between the waveguide core (n = 3.47) and the surrounding cladding (n = 1.45) ensures a small geometrical dimension of the waveguide [7,8]. The PIC design and microscope images of several key components are shown in Fig. 2.

Two different light coupling configurations used for sending and receiving measurement signals are shown in Fig. 3. A grating coupler and a 1×2 optical splitter are deployed in the first configuration (1gc), while two adjacent grating couplers are used in the second configuration (2gc). Both configurations can be used for receiving the reflected measurement light, though they still have several problems. The 1gc design suffers from a strong spurious reflection (the cross talk between the two left ports of the splitter, see Fig. 3) and a significant power loss (at least 6 dB) in the optical splitter. The cross talk problem is alleviated in the 2gc design since the two optical ports are not connected on chip. However, since the two grating couplers are spatially separated, the imaging system used for picking up the reflected light can not ensure a sufficient coupling efficiency in the backreflection. Note that the two grating couplers in the 2gc design are different because their common coupling direction is not perpendicular to the chip surface.

To estimate the receiving efficiency of the measurement signal, the phase in the measurement reflection is modulated during the measurement, by creating a vibration in the surface where the measurement light is focused. The amplitude of the vibration should be larger than $\lambda_0/2$ so that the maximum amplitude modulation depth is obtained. In practice, a piezo stack was used, driven by a 60 Vpp voltage signal oscillating at 31 Hz. According to the measured modulation depths, the power ratio of the reflected measurement signal to the reference signal was -28 dB for the 2gc LDV, and -34 dB for the 1gc LDV. This result indicates that the 2gc LDV is better than the 1gc LDV in terms of power efficiency.

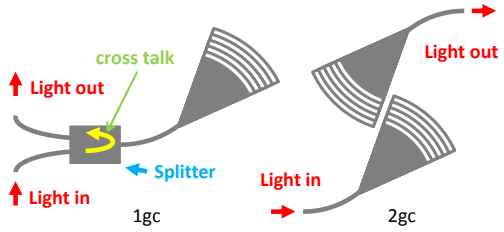

Fig. 3. The configuration of the 1gc type and the 2gc type light receiver.

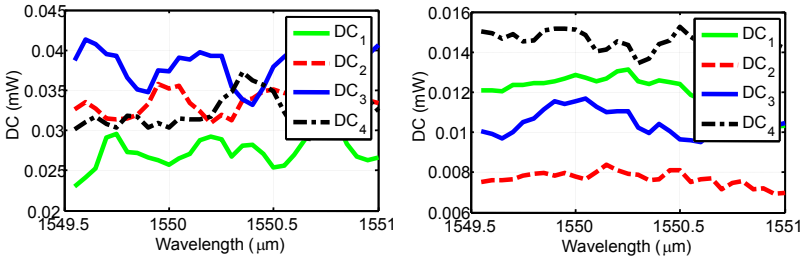

Fig. 4. (a) The average light power values at each output port (DC_j) for the homodyne 1gc LDV. (b) DC_j for the homodyne 2gc LDV.

#187527 - $15.00 USD Received 21 Mar 2013; revised 14 May 2013; accepted 16 May 2013; published 24 May 2013

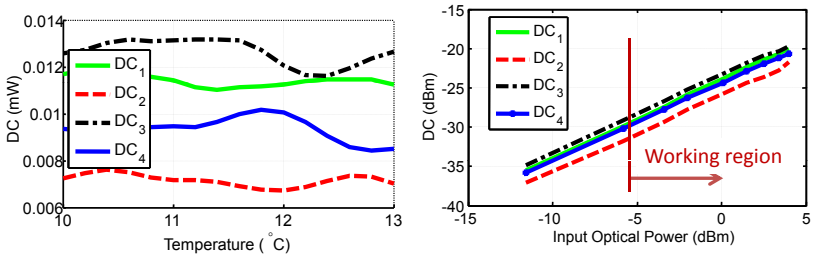

(a) (b)

Fig. 5. (a) The average light power values at each output port (DC_j) as a function of device temperature (2gc LDV). (b) DC_j as a function of the input power (2gc LDV).

To retrieve the values of the spurious reflections, the wavelength dependence of the photocurrent signals was measured. This was done by measuring the average values of the photocurrents for different wavelengths while the measurement signal is still under modulation. Since the reference signal and the spurious reflection have different optical lengths in the interferometer, an amplitude modulation is obtained in the average photocurrents and the corresponding modulation depth reveals the strength of the spurious reflection. The average optical power of each port (DC_j) is derived from the average photocurrent and plotted as a function of wavelength in Fig. 4(a) and Fig. 4(b). It is shown that the 2gc LDV has weaker DC signals than the 1gc LDV, but its modulation depths are also weaker than those of the 1gc LDV. The modulation depths indicate that the spurious reflection in 1gc LDV is about -25 dB lower than the reference signal, while that value in the 2gc LDV is lower than -30 dB. Alignment deviations may be responsible for the fact that the 1gc LDV had a larger DC value than the 2gc LDV.

Since the 2gc LDV picks up more back reflection and has less spurious reflection than the 1gc LDV, we will focus on the 2gc LDV in the following paragraphs. The differences between the 1gc and 2gc LDVs are summarized in Table 1.

The temperature stability of the PIC-based homodyne LDV with a 2gc light receiving component is also experimentally examined. The measured DC_j signals are shown in Fig. 5(a). The main cause for the deviations of these DC_j signals is the temperature-induced phase changes in the on-chip spurious reflections. These deviations are significant (up to 17%) as the temperature increases from 10°C to 13°C. In order to improve the performance of the PIC-based LDVs, we suggest to stabilize the chip temperature within 0.5°C by attaching a temperature stabilizer to the chip.

The relations between the input optical power value and the average light power values at the four outputs (DC_j) are shown in Fig. 5(b). By comparing the total optical power of the four outputs with the input optical power, it is found that the total loss of the optical power in the PIC-based LDV is around 18 dB. If the input light power is lower than -6 dBm, noise from the laser and the detectors would dominate and deteriorate the demodulation results.

Table 1. Performance of 1gc and 2gc LDVs, all values are compared with the light power of the reference light.

Type	measurement reflection (dB)	spurious reflection (dB)
1gc	-34	-25
2gc	-28	$<$-30

#187527 - $15.00 USD Received 21 Mar 2013; revised 14 May 2013; accepted 16 May 2013; published 24 May 2013

Homodyne LDVs are capable of measuring vibrations with large amplitudes and frequencies. The largest detectable amplitude and frequency are limited by the sampling rate of the analog-to-digital converter (ADC) and the speed of the DSP. With our present ADC which works with a sampling rate of 20 kHz, the maximal detectable velocity is around 7 mm/s. This value can be further increased once a higher sampling rate is used. This device can also be used to measure small vibrations (with an amplitude smaller than $\lambda_0/2$) if a temperature stabilizer is introduced and the active compensation approach for sub-half-wavelength vibrations is applied. In Fig. 6(a), the measured displacements of a piezo stack driven by two different oscillating voltage signals are shown. These two voltage signals have different peak-to-peak amplitudes, i.e. 60 Vpp and 5 Vpp, but the same oscillating frequency (31 Hz). These displacement values are calculated using the aforementioned "arc-tangent" algorithm. The vibration generated by the 5 Vpp voltage signal has an amplitude smaller than $\lambda_0/2$, but can still be measured with our active compensation approach for sub-half-wavelength vibrations. Their corresponding Lissajous curves and power spectral densities are also shown in Fig. 6(b) and in Fig. 7, respectively. It can be found that the measured power ratio between the two vibrations is around 20 dB. For the vibration driven by the 60 Vpp voltage signal, a signal-to-noise ratio (SNR) of around 50 dB is achieved. Derived from this SNR value, the minimal detectable vibration amplitude is around 6 nm, which corresponds to a peak velocity of 1.2 μm/s for this frequency.

4. Conclusions

We have reported an on-chip homodyne laser Doppler vibrometer (LDV), operating with a minimal input light power of around -6 dBm. Besides the noise in lasers and detectors, on-chip spurious reflection is the major source of deviation in these on-chip homodyne LDVs. With the help of an active compensation approach, the homodyne LDV is capable of measuring vibra-

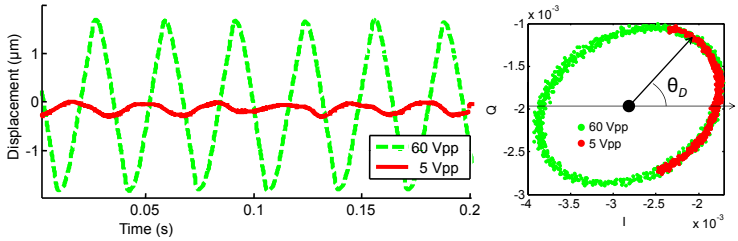

(a) (b)

Fig. 6. (a) Demodulated signals for two vibrations in time domain. (b) I&Q Lissajous curve.

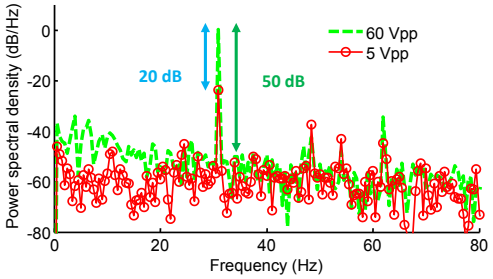

Fig. 7. Power spectral densities.

#187527 - $15.00 USD Received 21 Mar 2013; revised 14 May 2013; accepted 16 May 2013; published 24 May 2013

tions with amplitudes larger than one half of the light wavelength (775 nm). When measuring a sub-half-wavelength vibration, an extra temperature stabilizer and a specific active compensation approach for sub-half-wavelength vibrations are required. According to the measurement results, the minimal detectable amplitude of a 31 Hz vibration is around 6 nm, which corresponds to a velocity of 1.2 μm/s. In order to obtain a better measurement resolution and to further reduce the influence of on-chip spurious reflections, on-chip optical component designs with strongly reduced spurious back-reflections should be implemented in future work.

Acknowledgments

The authors acknowledge the Ghent University-Methusalem project "Smart Photonic Chips" for financial supports. The authors thank Lianyan Li for useful discussions.

#187527 - $15.00 USD Received 21 Mar 2013; revised 14 May 2013; accepted 16 May 2013; published 24 May 2013